Design and Practical Results of Four-CMG Cluster for Small Satellites

Seung Mok Lee*
Department of Satellite System and Application Engineering
University of Science and Technology, Daejeon, Korea 305-333

Hyun-Ho Seo and Seung-Wu Rhee*****
Korea Aerospace Research Institute, Daejeon, Korea 305-333

Abstract

This article presents the details of a designed control moment gyroscope (CMG) with a constant speed momentum wheel and one-axis-gimbal, and its experimental results performed at Korea Aerospace Research Institute. The CMG which is able to produce a torque of 100 mNm per each, is mounted in a pyramid configuration with four SGCMGs. Each CMG test and a single axis maneuver test with four-CMG cluster configuration are performed to confirm their performance on a ground-test facilities consisted of three major parts: a vibration isolation system, a dynamic force plate (Kistler sensor), and a DSP board. These facilities provide the accurate data of three axial and torques from the control moment gyro. Details of the CMG experimental results are presented with discussion of the experimental errors. The experimental data are compared with theoretical results and both results are used to verify their performance specifications.

Key Word : Control Moment Gyro, Four-CMG Cluster, Satellite Attitude Control

Introduction

A control moment gyro (CMG) is an actuator that produces a control torque by changing the angular momentum vector direction with respect to the spacecraft reference frame. The spinning rotor is mounted on a gimbal, and torquing the gimbal results in a precessional, gyroscopic reaction torque orthogonal to both the rotor spin and gimbal axes. The CMG is a torque amplification device because a small gimbal torque input produces a large control torque output on the spacecraft.[1]

There are two types of control moment gyros depending on the number of gimbal axes: single-gimbal control moment gyros (SGCMGs) and double-gimbal control moment gyros (DGCMGs). Depending on the wheel speed, and a CMG can be distinguished as either a constant-speed control moment gyros (CSCMGs) or a variable-speed control moment gyros (VSCMGs). The SGCMGs and CSCMGs in mechanical simplicity and higher output torque are the main consideration in this paper.

For full three axis control of a spacecraft, a cluster of four CMGs is normally used. Many different arrangements of CMGs [2-4] have been thoroughly studied in the past including four SGCMGs of of pyramid configurations and six parallel mounted SGCMGs and the CMGs have

* Graduate Student, University of Science and Technology
E-mail : smlee06@kari.re.kr Tel : 042-860-2686 Fax : 042-860-2898
** Researcher, Satellite Control System Team
*** Director, Satellite Future Technology R&D Division

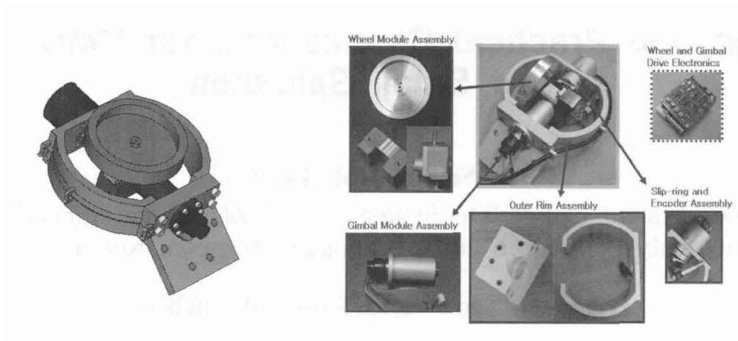

Fig. 1. Design of CMG

been employed before in various spacecraft mission such as NASA's Skylab, MIR, and ISS. Recently, smaller experimental SGCMGs in a pyramid configuration have been developed.[5-7] A four-SGCMG system of pyramid arrangement gives the advantage of having a spherical momentum envelop, which results to an almost equal momentum capability in all three axis.

A small four-SGCMG cluster depicted in Fig. 1, has developed by KARI.[8-11] This article focuses on designing and developing of the small four-CMG cluster and its experimental result for three axis control of a spacecraft. The work is summarized as follows: first, the design of each CMG and the four-CMG cluster are presented, and then a description of ground-test facility consisted of a vibration isolation system, a dynamic force plate, and a DSP board, is also presented. Details of the CMG experimental results are presented with discussions of the experimental errors. Also, this paper provides a practical insight into trying to measure the imbalance of the static mass of the gimbal axis on the ground-test facility under gravity influence.

Design of SGCMG

Description of Each CMG

Designing of CMG is a trade-off between angular momentum of flywheel, gimbal angle rate, output torque, mass and size and etc. Each module of CMG is composed of two motors constructed by Fauhaber. One motor is a stepper motor for the gimbal axis actuation and the other is a brushless DC motor with an integrated electronics for the flywheel axis actuation. The range of motion of the gimbal is not limited to rotate. Bearings support to each CMG and absolute encoders are used to provide measurements of the rotating gimbal of the CMG.

Each CMG produces a maximum output torque of 100 mNm along the CMG output axis with a maximum sustained angular momentum of 125 mNms at wheel speed 4000 RPM. The maximum gimbal rate is limited as ± 0.8 rad/s by the gear ratio of the gimbal stepper motor. Therefore the CMG output torque is given by,

$$\vec{M} = \vec{h} \times \vec{\delta} \tag{1}$$

$$\vec{h} = I_{wheel}\,\vec{\omega} \tag{2}$$

where $\vec{M}$ is the CMG output torque, $\vec{h}$ is the angular momentum vector of the flywheel at speed of 4000 RPM, I_{wheel} is the inertia of the flywheel, $\vec{\omega}$ is the flywheel angular rate vector of 4000 RPM, and $\vec{\delta}$ is the gimbal rate vector.

Design of Four-CMG Cluster

A typical pyramid mounting arrangement of four-CMG cluster is shown in Fig. 2. Four CMGs are constrained to gimbal on the face of a pyramid and gimbal axis are orthogonal to the

Table 1. Characteristics of CMG (per CMG)

Flywheel	3×10^{-4} kg-m^2 (Estimated)
Angular Momentum	0.125 Nms
Output Torque	0.1 Nm
Wheel Motor	Max. 15,000 RPM
Geared Gimbal Motor	Max. 0.8 rad/s
Range of Gimbal Motion	Infinite
Gimbal Angle Sensor	Abs. Encoder (16 bit)
Total Mass	1.56 kg
Dimension	200×138×60 mm

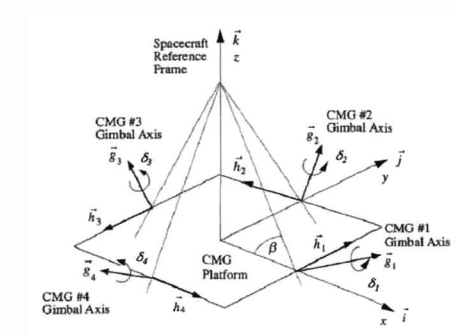

Fig. 2. Pyramid Arrangement

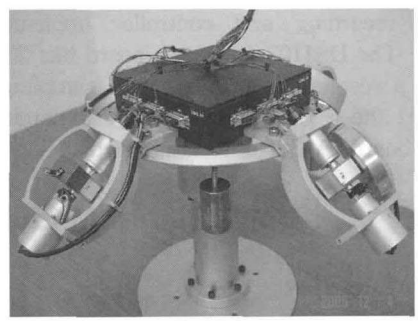

Fig. 3. Manufactured 4-CMG

pyramid faces. Each face is inclined with a skew angle of β from the horizontal, resulting in gimbal axis with a $(90-\beta)$deg inclination from the horizontal. Each CMG has same angular momentum and the skew angle is chosen as $\beta=57.9$deg. The manufactured configuration of four-CMG cluster is shown in Fig. 3.

Description of Ground-Test Facility

The ground-test facilities are consisted of three major parts: a vibration isolation system, a dynamic force plate (Kistler sensor), and a DSP board. The brief explanations of above experimental set-up are as follows. Also, these facilities are precisely described in Ref. [12].

Vibration Isolation System

The vibration isolation system is designed such that the dynamic force and torque of CMG

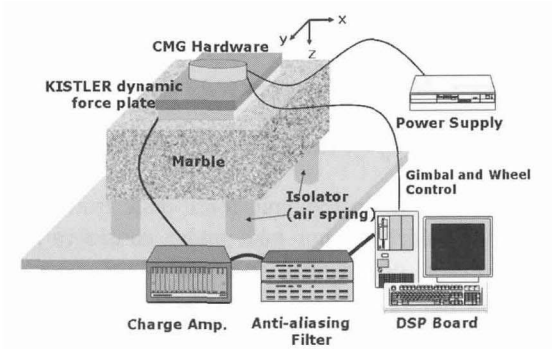

Fig. 4. Ground-Test Facility

hardware are isolated from the vibration of base excitation. Four active air spring systems are installed under a granite table as shown in Fig. 4.

Dynamic Force Plate (Kistler Sensor)

The Kistler multi-component force plate is designed to measure three orthogonal components of forces and torques simultaneously through inner twelve sensors. It has a gain of 1.1 at region of 300 Hz below and a resolution of 0.0001 N. The dynamic force plate is set up on the top of the vibration isolation system, and the CMGs were hard-mounted to the plate.

DSP Board

Typical DSP board (DS1103 from dSPACE) is used for real-time data monitoring, acquisition, recording and controller implementation with Control Desk via the MATLAB Simulink^{TM}. The DS1103 processor board has 20 channels of analog input and 8 channels of output. It supports a resolution of 16 bit with sampling frequency of maximum 1 MHz. An anti-aliasing filter follows the 6 DoF signals of the dynamic force plate so as to get clean signal in the data acquisition board. A 3th order Butterworth low pass filter was adopted to reduce input noise.

CMG Single Module Tests and Results

Single Module Test

Before characterizing four-CMG cluster, each of CMGs is tested on a dynamic force plate (Kistler sensor) to identify the level of torque noise. The experimental setup of each CMG and the dynamic force plate are depicted in Fig. 4.

Two experiments are conducted to identify the static characteristics of CMG set. The first experiment is that the angular momentum of flywheel sets to zero, $h_0 = 0$ as the gimbal rate $\dot{\delta}_y$, of 0.7 rad/s is issued. Mechanical disturbances due to stepper motor vibrations, misalignments, and static imbalances of gimbal axis are measured through this experiment. The second experiment is that the angular momentum of flywheel sets to 4000 RPM which is equivalent to $h_0 = 0.125\,Nms$ as $\dot{\delta}_y = 0.7 rad/s$ is issued. The maximum internal torque, τ_0 of each CMG with the specified commands can be calculated as

$$\tau_0 = 87.99\,mNm \tag{3}$$

Note the gimbal angle, δ_y is variable and the direction of angular momentum vector, h_0 is aligned with (-) x axis at the beginning in the test configuration. When the gimbal angle, δ_y is increasing in positive direction, the angular momentum vector can be expressed as

$$\vec{h} = \left[-h_0 \cos\delta \quad 0 \quad h_0 \sin\delta\right]^T \; mNms \tag{4}$$

Then, the measured output torque $\overrightarrow{M}$ can be represented under the current test configuration as

$$\overrightarrow{M} = \vec{h} \times \dot{\vec{\delta}} = \left[-\dot{\delta}_y h_0 \sin\delta_y \quad 0 \quad -\dot{\delta}_y h_0 \cos\delta_y\right]^T mNm \tag{5}$$

where $\overrightarrow{M}$ is the measured output torque in dynamic force plate frame. The experimental data are compared with theoretical results which do not take under considerations the wheel and gimbal motor dynamics, or any other internal disturbances such as motor cogging or torque ripple effects. The theoretical output torques in the case of the gimbal rate $\dot{\delta}_y = 10, 20, 30, 40\,\mathrm{deg}/s$ are shown in Fig. 5 respectively. Figs. 7-10 show the comparison results of the theoretical and experimental output torques for each CMG.

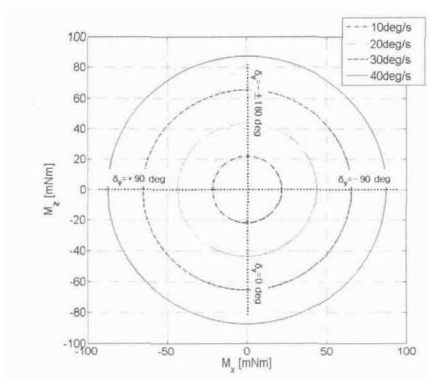

Fig. 5. Theoretical Output Torque per CMG

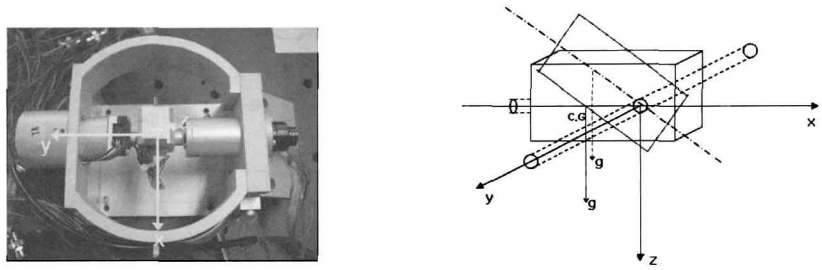

Fig. 6. Spin Motor Housing and Diagram

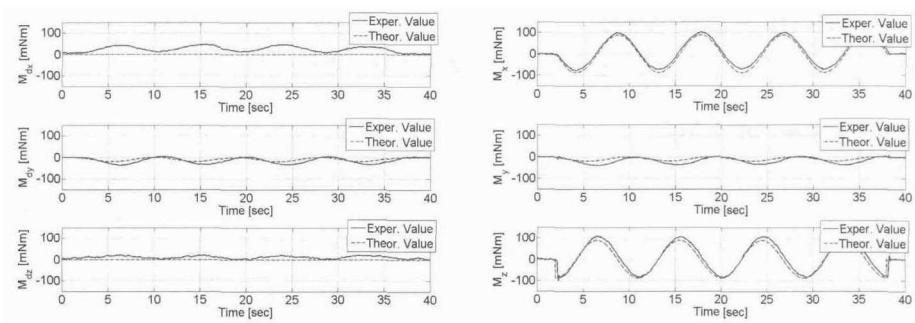

(a) Disturbance Torque (b) Output Torque

Fig. 7. Experiment of CMG #1

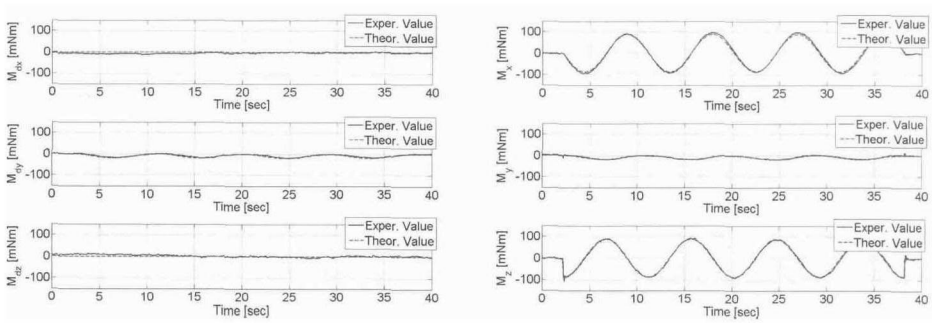

(a) Disturbance Torque (b) Output Torque

Fig. 8. Experiment of CMG #2

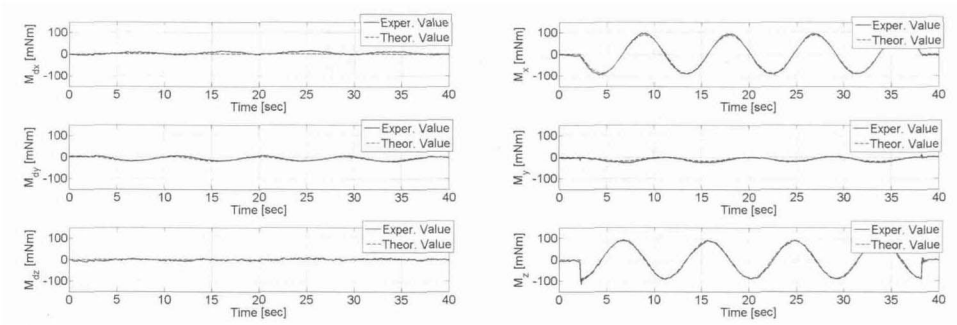

(a) Disturbance Torque (b) Output Torque

Fig. 9. Experiment of CMG #3

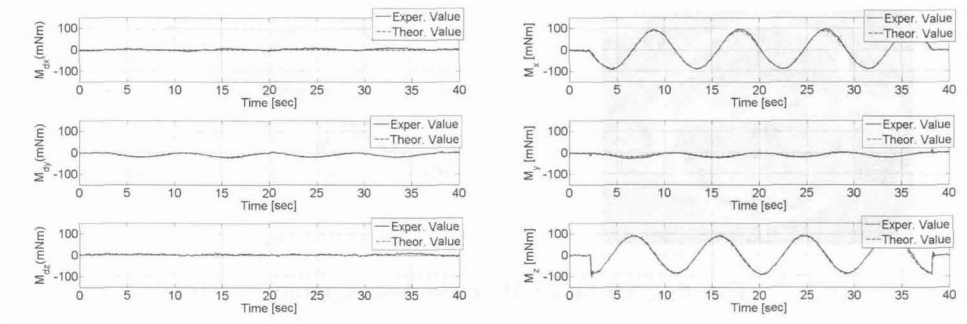

(a) Disturbance Torque (b) Output Torque

Fig. 10. Experiment of CMG #4

Experimental Errors of CMG

Analysis of the experimental results reveals that the main source of error between the theoretical and experimental, comes from the imbalance mass on the gimbal rotation axis. Physically, static imbalance is the offset of the center of mass of the gimbal from the axis of rotation. In this section, an analysis of the static imbalance mass of the gimbal is provided.

The measurements of the disturbance force in x axis and z axis can be used to estimate the static imbalance mass as seen in Eqs. (6)-(7) [13]

$$F_{dx} = U_s \bullet \dot{\delta}_y^2 \bullet \cos\left(\dot{\delta}_y t + \phi_x\right) \tag{6}$$

$$F_{dz} = U_s \bullet \dot{\delta}_y^2 \bullet \cos\left(\dot{\delta}_y t + \phi_z\right) \tag{7}$$

where U_s is the static imbalance. However, the disturbance forces from the static imbalance mass are small value relative to noise level because the maximum of the gimbal rate is limited as ± 0.8 rad/s. Therefore, trying to get more accurate results a practical approach to estimation of the imbalance of the static mass is presented. The static imbalance mass can be estimated from the measured disturbance torque in y axis M_{dy} which comes from the static imbalance effect of the gimbal axis with gravity influence. From the test configuration under gravity influence, M_{dy} can be expressed as

$$M_{dy} = U_s \bullet g \bullet \left(\cos\dot{\delta}_y t - 1\right) \tag{8}$$

where g is the gravity acceleration. As shown in Figs. 8-10, the range of disturbance torque in y axis is $0 \sim -20 mNm$. Thus, from Eq. (8), the estimated imbalance mass U_s is about $100 g_m cm$. The theoretical disturbance torque evaluated from the estimated value agrees with the experimental disturbance torques in y axis. The most imbalance of static mass comes from the spin motor housing imbalance shown in Fig. 6. In the case of CMG #1, the torque difference between theoretical and experimental result is larger than others as shown in Fig. 7. The most dominating source of the error is caused by mechanical misalignment due to the mistake in manufacturing process.

Four CMGs Tests and Results

Mathematical Modeling of Four CMGs

The fundamental principles of four-CMG cluster are briefly described here. The CMG angular momentum vector $\vec{H}$ is in general a function of CMG gimbal angle $\vec{\delta} = [\delta_1 \ \delta_2 \ \delta_3 \ \delta_4]$; i.e., we have

$$\vec{H} = \vec{H}(\vec{\delta}) \tag{9}$$

For the typical pyramid mount of four CMGs as shown in Fig. 2, the total CMG angular momentum vector $\vec{H} = [H_1 \ \ H_2 \ \ H_3]$ is easily expressed in spacecraft reference frame as,

$$\begin{aligned} \vec{H} &= \sum_{i=1}^{4} \vec{h}_i(\delta_i) \\ &= \vec{h}_1(\delta_1) + \vec{h}_2(\delta_2) + \vec{h}_3(\delta_3) + \vec{h}_4(\delta_4) \\ &= h_0 \begin{bmatrix} -\cos\beta\sin\delta_1 \\ \cos\delta_1 \\ \sin\beta\sin\delta_1 \end{bmatrix} + h_0 \begin{bmatrix} -\cos\delta_2 \\ -\cos\beta\sin\delta_2 \\ \sin\beta\sin\delta_2 \end{bmatrix} + h_0 \begin{bmatrix} \cos\beta\sin\delta_3 \\ -\cos\delta_3 \\ \sin\beta\sin\delta_3 \end{bmatrix} + h_0 \begin{bmatrix} \cos\delta_4 \\ \cos\beta\sin\delta_4 \\ \sin\beta\sin\delta_4 \end{bmatrix} \end{aligned} \tag{10}$$

and

$$\vec{\dot{\gamma}}_1 = \begin{bmatrix} \dot{\delta}_1 \sin\beta \\ 0 \\ \dot{\delta}_1 \cos\beta \end{bmatrix}, \ \vec{\dot{\gamma}}_2 = \begin{bmatrix} 0 \\ \dot{\delta}_2 \sin\beta \\ \dot{\delta}_2 \cos\beta \end{bmatrix}, \ \vec{\dot{\gamma}}_3 = \begin{bmatrix} -\dot{\delta}_3 \sin\beta \\ 0 \\ \dot{\delta}_3 \cos\beta \end{bmatrix}, \ \vec{\dot{\gamma}}_4 = \begin{bmatrix} 0 \\ -\dot{\delta}_4 \sin\beta \\ \dot{\delta}_4 \cos\beta \end{bmatrix} \tag{11}$$

where h_0 is the flywheel angular momentum, $\vec{h}_i$ is the angular momentum vector of the ith CMG expressed in spacecraft reference frame, $\vec{\dot{\gamma}}_i$ is the gimbal angular rate vector expressed in spacecraft reference frame, β is the pyramid skew angle, δ_i are the gimbal angle. The cross product of ith gimbal vector and angular momentum vector provides the torque generated per CMG. The sum of total CMG internal torques can then be obtained as,

$$\vec{\tau} \equiv \vec{\dot{H}} = \sum_{i=1}^{4} \vec{\dot{\gamma}}_i \times \vec{h}_i \tag{12}$$

Threrfore,

$$\vec{\tau} = h_0 \begin{bmatrix} -\dot{\delta}_1 \cos\beta\cos\delta_1 \\ -\dot{\delta}_1 \sin\delta_1 \\ \dot{\delta}_1 \sin\beta\cos\delta_1 \end{bmatrix} + h_0 \begin{bmatrix} \dot{\delta}_2 \sin\delta_2 \\ -\dot{\delta}_2 \cos\beta\cos\delta_2 \\ \dot{\delta}_2 \sin\beta\cos\delta_2 \end{bmatrix} + h_0 \begin{bmatrix} \dot{\delta}_3 \cos\beta\cos\delta_3 \\ \dot{\delta}_3 \sin\delta_3 \\ \dot{\delta}_3 \sin\beta\cos\delta_3 \end{bmatrix} + h_0 \begin{bmatrix} -\dot{\delta}_4 \sin\delta_4 \\ \dot{\delta}_4 \cos\beta\cos\delta_4 \\ \dot{\delta}_4 \sin\beta\cos\delta_4 \end{bmatrix} \tag{13}$$

where, $\vec{\tau}$ is the sum of total CMG internal torques in spacecraft reference frame.

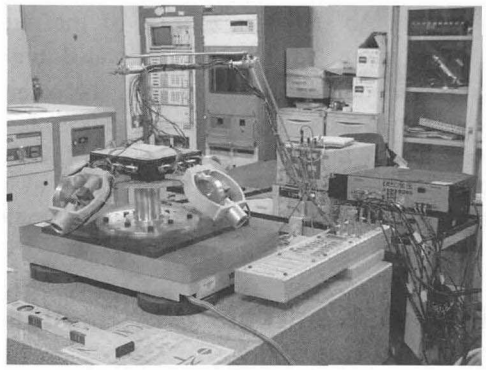

Fig. 11. CMG Cluster Experimental Setup

Single Axis Maneuver with Four CMGs

A maneuver to be investigated is, for a maneuver about z axis, a case in which, due to the CMG cluster arrangement, all four CMGs are used to complete the maneuver. The total CMG torque about the z axis can be calculated as, from Eq. (13)

$$\tau_z = \sum_{i=1}^{4} h_0 \dot{\delta}_i \sin\beta \cos\delta_i \tag{14}$$

Because of symmetric rotation $\delta_1 = \delta_2 = \delta_3 = \delta_4 = \delta$ and $\dot{\delta}_1 = \dot{\delta}_2 = \dot{\delta}_3 = \dot{\delta}_4 = \dot{\delta}$, the torque generated four-CMG cluster about z axis can be calculated as,

$$\tau_z = 4h_0 \dot{\delta} \sin\beta \cos\delta \tag{15}$$

To verify the z axis output torque, the command profile of gimbal rate for the z axis maneuver test is defined as,

$$\dot{\delta} = \begin{cases} 0 & \text{for} \quad t < 1s \\ 0.35\, rad/s & \text{for} \quad 1 \le t < 5s \\ -0.35\, rad/s & \text{for} \quad 5 \le t < 9s \\ 0 & \text{for} \quad t > 9s \end{cases} \tag{16}$$

The maneuver performed is an open-loop maneuver by four stepper motors. As shown in Fig. 12, $\tau_z = 139.6\, mNms$ is obtained with $\dot{\delta} = 0.35\, rad/s$ and $\delta = 0\,\text{deg}$, $h_0 = 125\, mNms$. It is observed that the output torque, M_z is increasing as the gimbal angle, δ is increasing as seen in Fig. 12 because the z axis component of angular momentum in body frame is increasing.

The previous maneuver represents a single axis maneuver about the z axis, with the configuration of CMG cluster. The next test to be performed is for a maneuver about the x axis and y axis. Because of a typical configuration, $\dot{\delta}_1 = -\dot{\delta}_3 = \dot{\delta}$, $\dot{\delta}_2 = \dot{\delta}_4 = 0$ and $\delta_1 = -\delta_3$: a pair of CMGs among the four CMGs are used. Thus, the generated x axis torque of four CMG cluster can be obtained as,

$$\tau_x = -2h_0 \dot{\delta} \cos\beta \cos\delta \tag{17}$$

The torque and gimbal profiles of the test result are shown in Figs. 13-14.

After performing a similar derivation for the τ_y with a rotation of $\dot{\delta}_2 = -\dot{\delta}_4 = \dot{\delta}$, $\dot{\delta}_1 = \dot{\delta}_3 = 0$ and $\delta_2 = -\delta_4$, τ_y can be obtained as,

$$\tau_y = -2h_0 \dot{\delta} \cos\beta \cos\delta \tag{18}$$

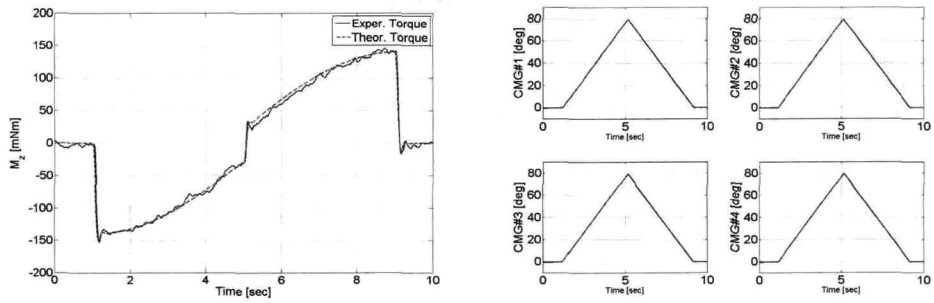

(a) CMG Output Torque (b) Gimbal Angles

Fig. 12. Z Axis Maneuver

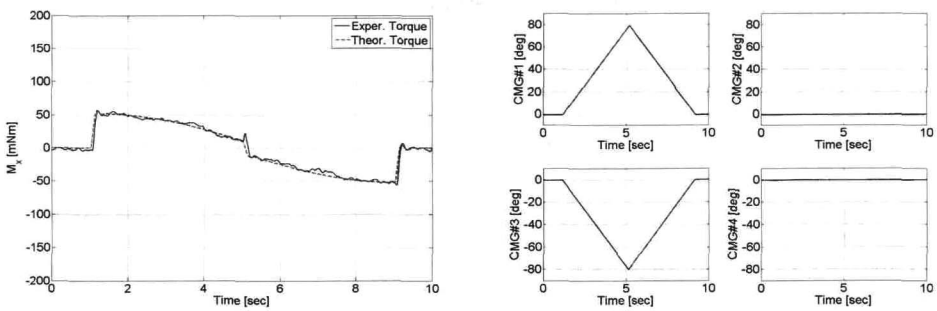

(a) CMG Output Torque (b) Gimbal Angles

Fig. 13. X Axis Maneuver

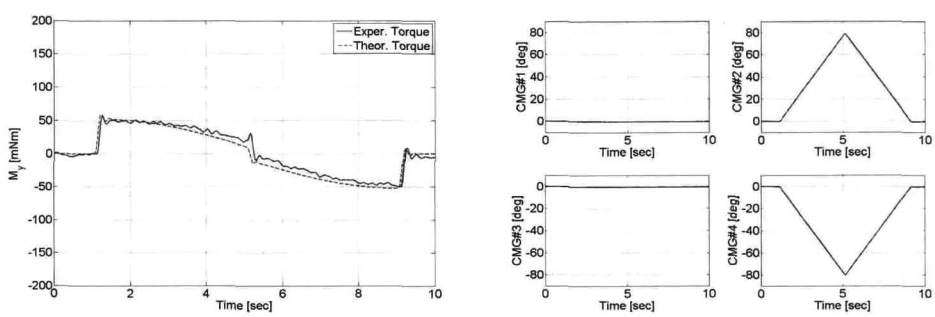

(a) CMG Output Torque (b) Gimbal Angles

Fig. 14. Y Axis Maneuver

The command profile of gimbal rate for the maneuver are same as Eq. (16). The maximum torque, $\tau_x = \tau_y = 52.35\, mNms$ with $\dot{\delta} = 0.35\, rad/s$ and $\delta = 0\,\mathrm{deg}$, $h_0 = 125\, mNms$ is obtained as shown in Figs. 13-14. The four-CMG cluster body frame coincide with the dynamic force plate frame. Since the dynamic force plate measures the reaction torque of CMG, the sign of internal torque $\vec{\tau}$ is opposite to the measured torque $\vec{M}$. Due to the symmetrical arrangement of the CMGs and Eqs. (17), (18), the output torques of the two maneuvers should be equally generated. However, the torque difference between theoretical and experimental values about the y axis is larger than one about the x axis. The main source of the torque difference between theoretical and experimental results is caused by mechanical misalignments on the CMG cluster arrangement of pyramid-type.

Conclusions

The details of experimental results for control moment gyros for agile small satellites are presented. Using ground-test facilities, such as vibration isolation system, dynamic force plate (Kistler sensor), DSP board, and anti-aliasing filter and etc, ground experiments were performed successfully to verify the performance of the designed single-gimbal control moment gyro. It is demonstrated that each CMG is able to generate the output torque of 100 mNm as designed. The torque test results of CMG cluster are provided in x axis, y axis, z axis of the four-CMG cluster to verify whether the output torque of cluster is same as expected: four CMGs are mounted on typical pyramid arrangement with skew angle $\beta = 57.9$. Analytical results are also provided to compare with the experimental results. Having a total mass of about 7.5 kg (including all electronics), four-CMG cluster were shown in a practical way potentially to be an efficient and highly capable means of controlling agile small satellites.

Acknowledgement

The first author expresses his thank to the kindness of satellite control team members in KARI to allow using his test facility to perform the test.

References

1. Wie, B., Space Vehicle Dynamics and Control, AIAA Education Series, AIAA, Reston, VA, 1998, pp. 435-439.

2. Chubb, W. B., and Epstein, M., "Application of Control Moment Gyros to the Attitude Control of the Apollo Telescope Unit," Proceedings of AIAA Guidance, Control, and Flight Mechanics Conference, AIAA, New York, 1968.

3. Ross, C. H., and Worley, E., "Optimized Momentum and Attitude Control System for Skylab," Proceedings of AIAA Guidance, Control, and Flight Mechanics Conference, AIAA, New York, 1971.

4. Roser, X., and Sghedoni, M., "Control Moment Gyroscopes (CMG's) and Their Application in Future Scientific Missions," Proceedings of 3rd International Conference on Spacecraft Guidance, Navigation and Control Systems, 1997, pp. 523-528.

5. Lappas, V., Steyn, W., H., and Underwood, C., "Attitude Control for Small Satellites Using Control Moment Gyros," Acta Astronautica, Vol. 51, No. 1-9, 2002, pp. 101-111.

6. Lappas, V., Steyn, W., H., and Underwood, C., "Design and Testing of a Control Moment Gyroscopes Cluster for Small Satellites," Journal of Spacecraft and Rockets, Vol. 42, No. 4, 2005, pp. 729-739.

7. Jung, D., and Tsiotras, P., "An 3-DoF Experimental Test-Bed for Integrated Attitude Dynamics and Control Research," AIAA Guidance and Navigation, and Control Conference, Austine, Texas, 2003, AIAA 2003-5331.

8. Seo, H. H., "Steering Law Realization and Hardware Implementation of Single Gimbal Control Moment Gyroscopes for Agile Spacecraft," M.S. Thesis, University of Science and Technology, Daejeon, Korea, Feb, 2006.

9. Lee, S. H., Rhee, S. W., Oh, S. H., Yong, K. L., Kim, K. W., and Seo, H. H., "Development of Miniature CMG for Satellite Attitude Control (I): Design & Manufacture," Proceeding of the 2005 KSAS Fall Conference, KSAS05-2705, pp. 878-881.

10. Seo, H. H., Rhee, S. W., Lee, S. H., Oh, S. H., and Kim, H. J., "Development of Miniature CMG for Satellite Attitude Control(Ⅱ): Experimental Setup and Performance Test," Proceeding of the 2005 KSAS Fall Conference, KSAS05-2706, pp. 882-885.

11. Seo, H. H., Rhee, S. W., Lee, S. H., Oh, S. H., Yim, J. R., and Kim, H. J., "Arrangement and Hardware Test of Single Gimbal Control Moment Gyroscopes Cluster," Proceeding of the 2006 KSAS Spring Conference, KSAS06-1811, pp. 840-844.

12. Oh, S. H., and Rhee, S. W., "Micro-Vibration Measurement, Analysis and Attenuation Techniques of Reaction Wheel Assembly in Satellite," Journal of The Korean Society for Aeronautical and Space Sciences, Vol. 30, No. 8, 2002, pp. 126-132.

13. Masterson, R. A., Miller, D. W., and Grogan, R. L., "Development of Empirical and Analytical Reaction Wheel Disturbance Models," 1999, AIAA-99-1204.